学位論文要旨

Study on effects of electric field on optical electron-spin injection into InGaAs quantum dots

陳　　杭

CHEN　Hang

Contents

1. Introduction

Self-assembled quantum dots (QDs) of III–V compound semiconductors have been extensively investigated [1, 2] owing to their unique and highly useful electronic properties, including significant suppression of carrier or exciton spin relaxation in addition to strong three-dimensional (3D) quantum confinements [3, 4, 5, 6]. Besides, these self-assembled QDs become an excellent candidate for the development of next-generation Light-emitting diode (LED) with a property of ultra-low energy consumption [7, 8].

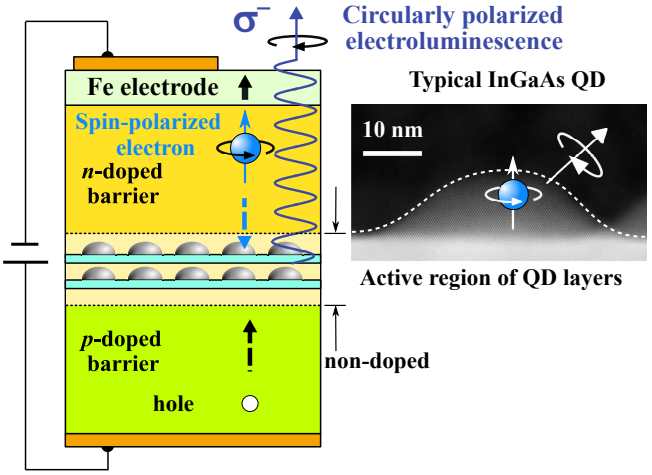

Figure 1. Schematic drawing of a QD-based spin-polarized LED structure with self-assembled InGaAs QDs in the active region. A typical cross-sectional TEM image of InGaAs QD is shown in right.

For the practical use, high-density QDs are known to achieve efficient spin injection performance owing to suppression of Pauli spin blocking [9, 10], as well as high optical gains [11, 12]. Injection of spin-polarized carriers from the spin aligner into the active region is essential for realizing spin functional photoelectrical devices such as a spin-polarized LED [13]. Bulk semiconductors or quantum wells (QWs) were used as active regions in the spin-LED [14]. However, the spin injection was not efficient because of the spin relaxation during the injection process in addition to the spin relaxation in the active region after the injection, particularly at high temperatures. Spin-relaxation times in these devices are in general very fast due to their 3D or 2D characters of bulk or QW active regions, in addition to the 3D barriers [15]. However, in the QD-based spin-LED, the major spin-relaxation mechanism should be inactive [16, 17, 18]. Recently, QD-based spin-LEDs have been reported, which utilize QD-based active layers typically as shown in Fig. 1 [15, 19]. An injection spin polarization of 5% in QDs was measured [19].

The spin-polarized electrons are injected into the QD-based active region and then circularly polarized lights can be emitted by recombination with un-polarized holes owing to the optical selection rule.

2. Research Purpose

Improving the spin injection efficiency into the QD-based spin-LED is a subject of intense research. Therefore, a spin injection process with the spatial transfer from a QW into QDs has been introduced to improve the spin-capturing efficiency. For this purpose, a QW/QDs tunnel-coupled nanostructure was proposed [20].

In this QW/QDs coupled nanostructure, a QD layer was coupled with an adjoining QW through a thin tunneling barrier (Fig. 2).

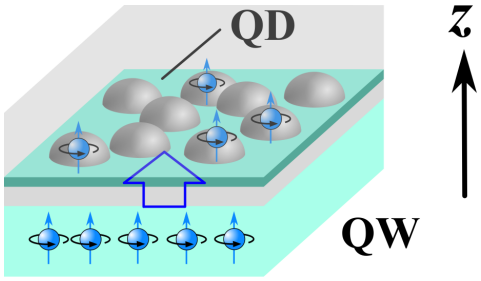

Figure 2. Schematic drawing of the QW/QD coupled nanostructure.

This tunnel-coupled QW/QDs nanostructure is expected to efficiently capture electron spins prior to spin relaxation, while electrons with lighter effective masses can be usually injected into QDs by Auger scattering or using electron blocking layers in layered device structures [21]. Our previous studies of QW/QDs nanostructures revealed an efficient and ultrafast spin injection with injection time constants ranging from 5 to 20 ps that maintain high degrees of spin polarization ($> 90\%$) during tunneling from the QW to QD. Coupled states and the resultant spin injection from the 2D QW into 0D QDs are of interest due to the spin-conserving tunneling nature between these different dimensionalities [21, 22, 20]. With increasing temperature up to 200 K, this spin-transfer dynamics was not affected; thus, the QW/QDs coupled nanostructures will promote the development of room-temperature device operation [20, 23].

As shown in Fig. 3, the optical spin injection from the 2D-QW in to 0D-QDs shows three advantages in this subject [21]: First, more than 50% initial spin polarization of excitons can be generated in the QW; Second, spin injection from the QW into QDs across the barrier can be ultrafast when the barrier is sufficiently thin; Last, the spin relaxation can be suppressed due to strong 3D quantum confinements in the QDs after the injection.

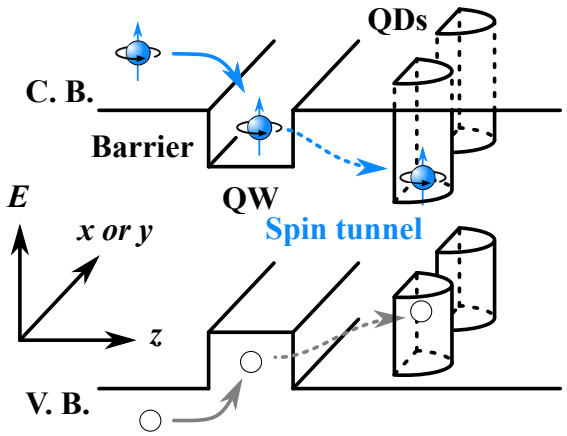

Figure 3. Schematic drawing of the band-structure and possible capture process of electron spins in the QW/QD coupled nanostructure.

To apply this interesting QW/QDs coupled nanostructure to spin functional optical devices, effects of electric field on the spin dynamics should be investigated in detail. The tunnel-coupled QD-QW potentials can be precisely tuned by applying external electric fields along the growth direction. Therefore, the tunneling spin injection dynamics can be controlled by the electric field. Electric field control of the spin injection dynamics and the resultant spin states in high-density QDs will provide an effective approach exploring efficient spin injection through highly spin conserving resonant spin tunneling, which is potentially applied to semiconductor spintronics such as spin-polarized optical devices. Besides, we have observed both positive and negative trion formations with opposite electron spin directions in the QD ground states. This negative trion formation can significantly suppress the degree of circular polarization as a result of those spectral overlapping with opposite circular polarizations depending on the spin directions [24]. Therefore, the selective formation of positive and negative trions utilizing electric-field applications is also of great interest. This has a potential to enhance injected spin polarizations where the ratio of the number of electron and hole injections from a QW-based spin reservoir can be controlled by an electric field modification of the coupled QD-QW potential.

3. Experimental Procedures

3.1 Layered QD-based sample and device structures

In this study, optical active layers composed of coupled QW/QDs coupled nanostructures of InGaAs were grown by molecular beam epitaxy. Figure 4 shows a sample structure with the coupled QD-QW optical active layer. Non-doped GaAs layers with a 100-nm-thick $Al_{0.1}Ga_{0.9}As$ barrier were grown at 580°C on a *p*-doped GaAs (001) substrate. An $In_{0.1}Ga_{0.9}As$ QW with a thickness of 20 nm and a GaAs tunneling barrier with a thickness of d_B were then grown at 520°C. The substrate temperature was subsequently decreased to 500°C and a self-assembled $In_{0.5}Ga_{0.5}As$ QD layer was grown. This QD layer was capped with a 10-nm-thick GaAs. Besides, a *p*-doped QD sample was prepared with Be in this capping layer, which will be described later. These QD-QW optical active layers were covered at 580°C by a top 60-nm-thick $Al_{0.2}Ga_{0.8}As$ barrier capped with a 10-nm-thick GaAs. The top and bottom AlGaAs barriers ensure that carriers are condensed in proximity to the QD-QW active layer, in addition to suppressing a current flow. A Ti/Au electrode was deposited on the top of this semiconductor layered structure and a 10-μm-square optical window was fabricated enabling optical spin excitations and PL observations. The average base diameter and height of the QDs were 20 and 5 nm, respectively, with a high areal density of 5.5×10^{10} cm^{-2}.

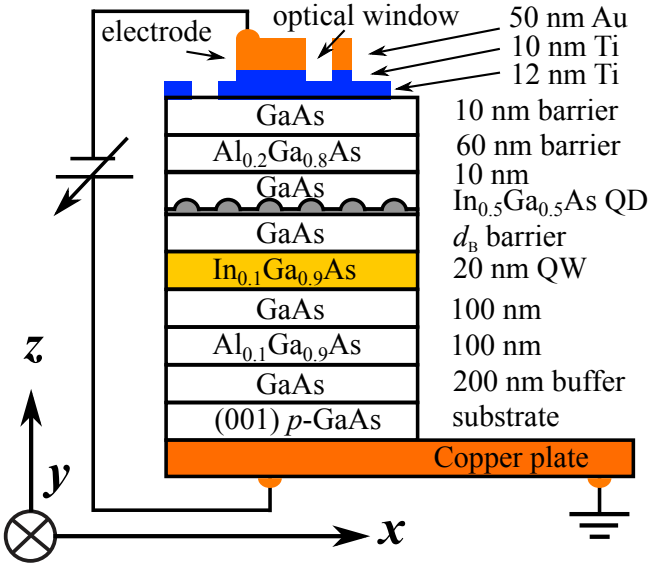

Figure 4. Schematic drawing of the electric-field-effect optical device structure with an optically active layer of the non-doped QW/QDs coupled nanostructure.

Figure 5 (a) shows a schematic drawing of the device operation using an optically active layer of the coupled QW/QDs nanostructure. The coupled potentials as a function of the electric field were also calculated. Spin-polarized carriers were initially excited in the QW selectively by irradiating circularly polarized lights with a specific energy slightly above the QW bandgap. Subsequently, the injected spin states via tunneling can be detected as a function of electric field by observing circularly polarized PL from the QDs, which obeys the optical selection rule [25], as shown in Fig. 5 (b). The effect of *p*-doping in the QDs was also examined to investigate trion formation in the spin injection process.

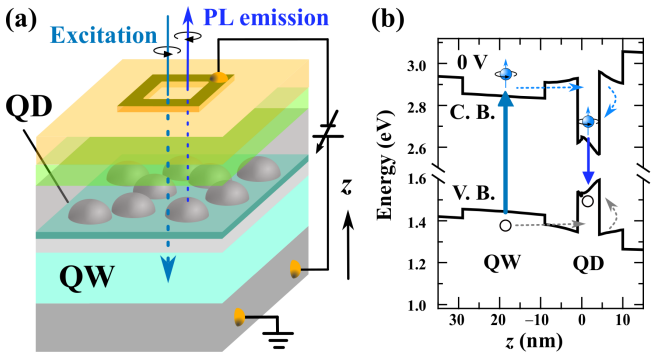

Figure 5. (a) A schematic drawing of optical spin generation and detection in the non-doped coupled nanostructure controlled by an electric field. (b) An example of the 3D-calculated potential with a barrier thickness of $d_B = 8$ nm at a bias voltage of 0 V along the growth direction (z-axis) of the coupled InGaAs QW/QDs nanostructure grown on a p-doped GaAs substrate, and the resultant electron-spin injection process.

3.2 Optical measurement

Figure 6 shows a conventional micro-photoluminescence (μ-PL) measurement setup used in this study. The samples were set at 4 K on a cold-finger of the cryostat. The excitation was made using σ^- circularly polarized lights selectively for the QW at 1.459 eV. This energy was above the QW bandgap while sufficiently below a GaAs-barrier bandgap of 1.519 eV. A mode-locked Ti:Sapphire pulsed laser with a repetition rate of 80 MHz and a temporal width of 150 fs was also used as the excitation source for time-resolved μ-PL measurements. The circular polarization degree (CPD) of excited electrons in the QW is expected to be 50–100% depending on the degree of hole mixing, where heavy and light holes can be excited by the above femtosecond laser with a relatively broad spectral width of 22 meV.

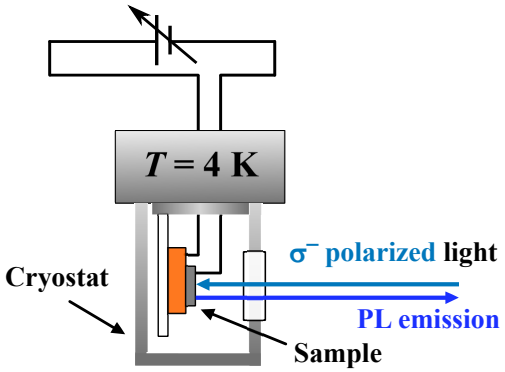

Figure 6. Schematic drawing of a μ-PL setup.

A focused laser beam was irradiated on the sample surface, which was set onto a cold-finger of the liquid-He flow type cryostat. The QD-PL emission from the sample was collected through an objective lens (× 20) with a numerical aperture of 0.35. A combination of circular polarization filter with a linear polarization one and some pass filters were used for the detection of circular polarization property of PL. QD-PL emissions were corrected and introduced to a monochromator, and then detected by a highly sensitive CCD cooled by liquid-nitrogen. An external bias along the growth direction [z-direction in Fig. 5 (a)] of the semiconductor layers was applied, ranging between −3 and +3 V.

Time-resolved PL (TRPL) was also measured at 4 K by using time-correlated single-photon counting (TC-SPC) with a time resolution of 40 ps.

4. Efficient electron-spin injection into QD by electric field application

4.1 QD-PL behavior

Figure 7 (a) shows a typical contour plot of the QD-PL intensity as functions of photon energy and bias voltage, in a device sample with a QW/QDs coupled active layer without p-doping and with a tunneling barrier thickness (d_B) of 8 nm. The PL energies exhibiting intense PL, ranging from 1.24 to 1.32 eV, correspond to the QD ground states (GSs) of the QD ensemble. Above 1.32 eV, the PL from the excited states (ESs) is observed; however, its intensity is rather weak under this excitation power.

Figures 7 (b)-(d) show calculated potentials around the QW/QDs coupled nanostructure along the growth direction with external biases of −1.5 V, 0.5 V, and +2.0 V, respectively. As shown in Fig. 7 (a), the contour plot of un-doped QD-PL intensity can be divided into 3 areas: (i), (ii), and (iii), as shown in the figure. These three bias areas are characterized as follows: (i) The PL intensity decreases with increasing negative bias toward −2.0 V. This result can be attributed to hole localization opposite from the QD side in the QW, as shown in Fig. 7 (b). This localization of hole in the QW apart from the QD side weakens the QD-PL intensity. (ii) The PL intensity increases significantly above 0 V and shows a maximum around 1 V, indicating efficient carrier injection from the QW into the QDs by tunneling, as shown in Fig. 7 (c). (iii) Above 1 V, the PL intensity decreases again, where electrons can be likely confined to one side of QW opposite from the neighboring QD layer, as shown in Fig. 7(d). These changes can be caused by electric-field-induced band bending.

The QD-PL spectrum with an excitation power of 320 μW at the bias voltage of 1.0 V is shown in Fig. 8, compared to that with a sufficiently lower excitation power of 10 μW (a light blue dotted line). The QD-PL spectrum with the latter 10 μW excitation indicates the inhomogeneous GS distribution in this high-density QD ensemble sample. The peak energy of the QD-PL

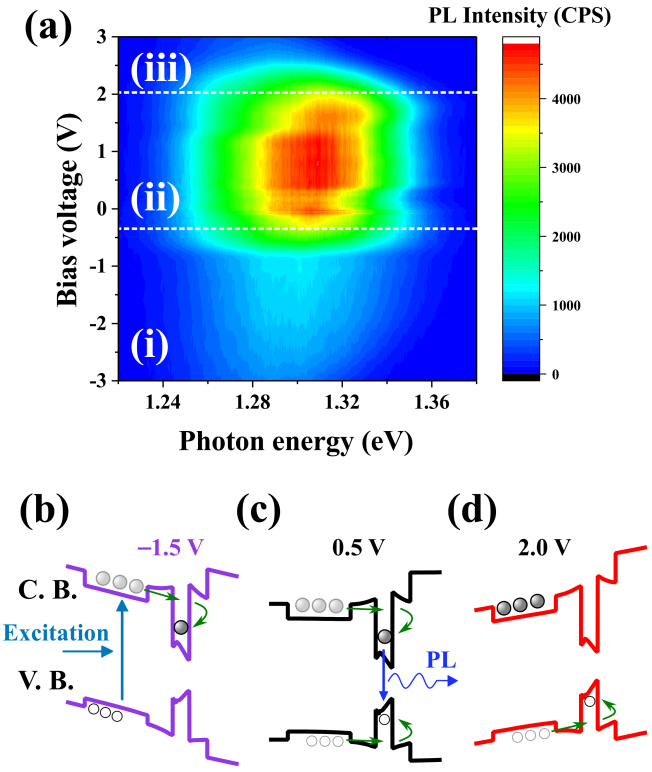

Figure 7. (a)A contour plot of PL intensity at 4 K from un-doped QDs with $d_B = 8$ nm as functions of photon energy and bias voltage under an excitation laser power of 320 μW. 3D-calculated potentials as a function of growth direction (z-axis) in the coupled QW/QDs nanostructure with bias voltages of -1.5 V (b), 0.5 V (c), and 2.0 V (d), where the carrier dynamics after photo-excitation in the QW are schematically illustrated.

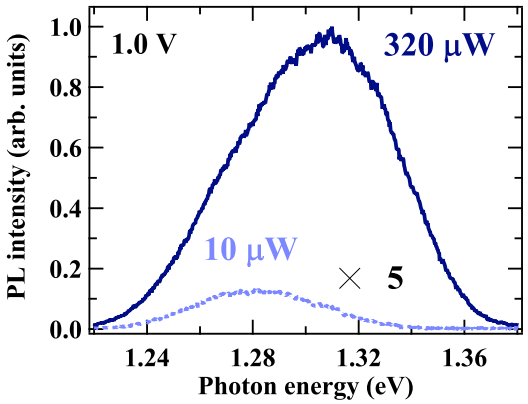

Figure 8. QD-PL spectra with 1.0 V under excitation powers of 320 μW (a dark blue solid line) and 10 μW (a light blue dotted line) in the sample with $d_B = 8$ nm.

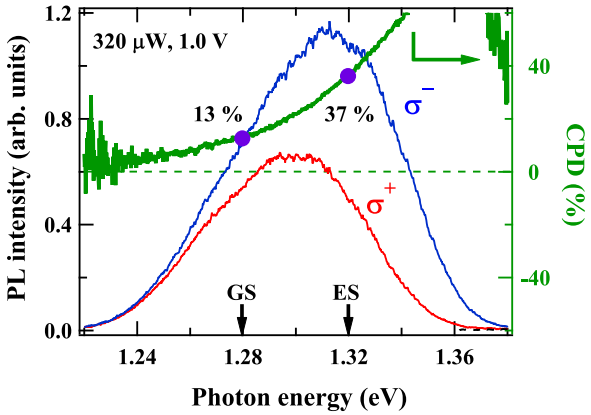

Figure 9. Circularly polarized PL spectra (co-circular σ^-; a blue line, cross-circular σ^+; a red line, and the corresponding CPD value; a green line) under σ^- excitation at 4 K with 1.0 V in the un-doped QD sample ($d_B = 8$ nm). Purple closed-circle marks indicate CPD values corresponding to the GS and ES energy peaks in the QD-PL, respectively.

spectrum with an excitation power of 320 μW shifts to the higher-energy side due to a state filling effect in this QD ensemble.

4.2 Circularly polarized QD-PL spectra

Figure 9 shows circularly polarized PL spectra for the un-doped QD sample with $d_B = 8$ nm, under an excitation power of 320 μW and a bias voltage of 1.0 V. A co-circular (σ^-) spectrum for the excitation polarization is plotted using a blue line, while cross-circular (σ^+) one is shown by a red line.

This circularly polarized PL was detected from the QDs after the carrier (spin) injection from the QW. The CPD reflecting the electron spin polarization at emissive states is expressed by:

$$\mathrm{CPD} = (I_{\sigma-} - I_{\sigma+})/(I_{\sigma-} + I_{\sigma+}), \quad (1)$$

where $I_{\sigma\mp}$ is left- or right-handed ($\sigma^\mp$) circularly polarized QD–PL intensities after σ^- excitation for the QW. The corresponding QD-CPD value obtained from the QD-PL spectra is also plotted as a function of photon energy, as a green line in Fig. 9.

A positive CPD property (co-circular; parallel spin to the initial QW spin) is dominant even at GSs with 1.0 V in Fig. 9. With an increase of photon energy, the value of CPD increases from 13% at GS (1.28 eV) up to 37% at ES (1.32 eV).

4.3 CPD value of QD-PL

Figure 10 shows contour plots of the CPD value in the un-doped QD-PL, under excitation powers of 10 μW and 320 μW. These contour plots of CPD are composed of a series of QD-CPD value as functions of photon energy and bias. The circularly polarized PL reflecting carrier spin states shows the following properties.

Positive CPD values ranging from 10% to 30% are observed above 0.2 V around the PL-intensity peak, in-

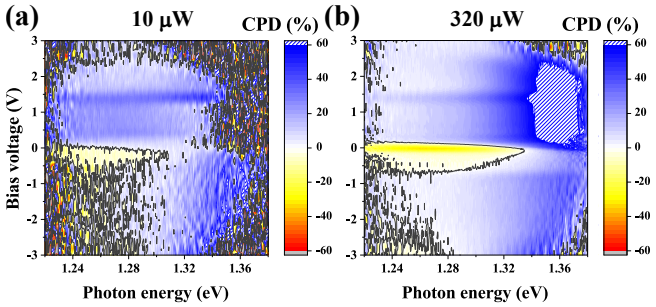

Figure 10. Contour plots of a CPD value at 4 K as functions of photon energy and bias voltage under excitation powers of 10 μW (a) and 320 μW (b), for the un-doped QD sample with $d_B = 8$ nm.

dicating a parallel spin state to the initial spin direction in the QW. A higher energy side corresponding to the QD-ESs exhibits higher CPD values. These co-circular PL characteristics clearly show efficient spin injection from the 2D-QW to 0D-QDs in this coupled nanostructure [23, 20]. As can be seen in Fig. 10 (b), high positive (CPD) values greater than 60%, indicating highly efficient injection, are observed ranging from 0 to 2.5 V under 320 μW.

In contrast, I find a clear bias region from −0.7 to 0.1 V exhibiting negative CPD values in Fig. 10 (b). This phenomenon of negative CPD will be discussed in the next chapter.

5. Electric-field effects on spin-injection polarity and the spin-polarization degree in QD

5.1 Electric-field effects on electron-spin polarity during spin injection

Figure 11 shows circularly polarized PL spectra for the un-doped QD sample with an excitation power of 320 μW under bias voltages of 0 (a) and 1.0 V (b). Significant negative CPD (cross-circular, anti-parallel spin to the initial QW spin) values down to −29% are observed only at the GSs with 0 V, as shown in Fig. 11 (a), while the ESs above 1.33 eV show positive CPDs (co-circular, parallel spin resulting from efficient spin injection). In contrast, a positive CPD property (co-circular, parallel spin) is dominant even at the GS with 1.0 V, as shown in (b).

A clear bias region from −0.7 to 0.1 V exhibiting negative CPD values can be observed, which was mentioned in the previous chapter. This indicates an anti-parallel spin state in the QDs against for the initial QW-spin direction. These negative CPDs disappear at the higher energy side corresponding to the ESs.

Circularly polarized transient PL and the corresponding CPD from the QD-GS are shown with a bias voltage

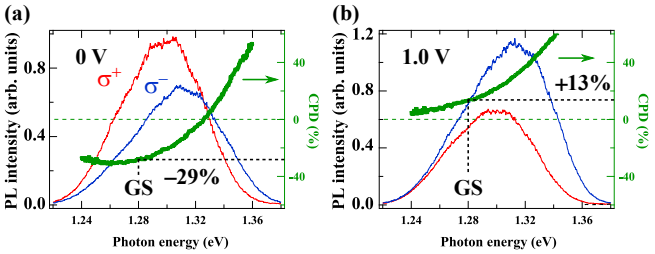

Figure 11. Circularly polarized PL spectra (co-circular σ^-: a blue line, cross-circular σ^+: a red line, and the corresponding CPD value: a green line) at 4 K under σ^- excitation for the QW with 0 V (a) and 1.0 V (b).

of 0 V [Fig. 12 (a)] and 1.0 V [Fig. 12 (b)]. A drastic change in the time-dependent CPD property is observed at this bias condition. Significant negative CPD values gradually develop from almost 0 at the beginning to −40% after 2.0 ns. In contrast, marked initial positive polarizations up to 30% appear at 1.0 V and then decrease steeply within 0.2 ns.

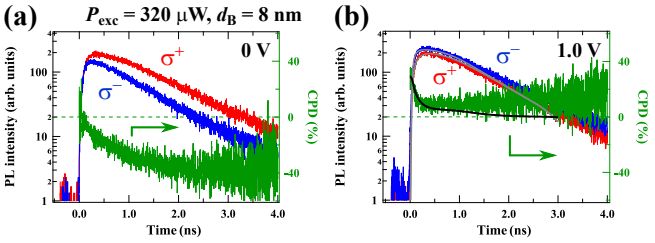

Figure 12. Circularly polarized time-resolved PL responses at the GS (1.28 eV) in the un-doped QD sample, at 4 K with 0 V (a) and 1.0 V (b) under the QW-σ^- excitation of 320 μW.

Negative CPD (cross-circular polarization) properties were previously observed by formation of negatively charged excitons (trions) with excess electrons in QDs [24, 26, 27], while positively charged trions with excess holes can show co-circular polarization. Several mechanisms based on the negative trion formation have been proposed to explain the negative PL polarization. A spin flip-flop transition via electron-hole scattering at ESs in QDs was discussed [26]. The relatively slow development of the negative CPD as shown in Fig. 12 was also observed in the negative trion formation phenomenon [26, 27]. An effect of dark exciton accumulation was also reported by capturing the dark excitons. Effects of excitation power density and p-doping were studied, where higher excitation powers enhanced a negative CPD value and that enhancement correlated with increasing emission intensity from the ESs [27].

Here, I briefly explain how the negative PL-CPD arises in our QW/QD samples, depending on the electric

field [26].

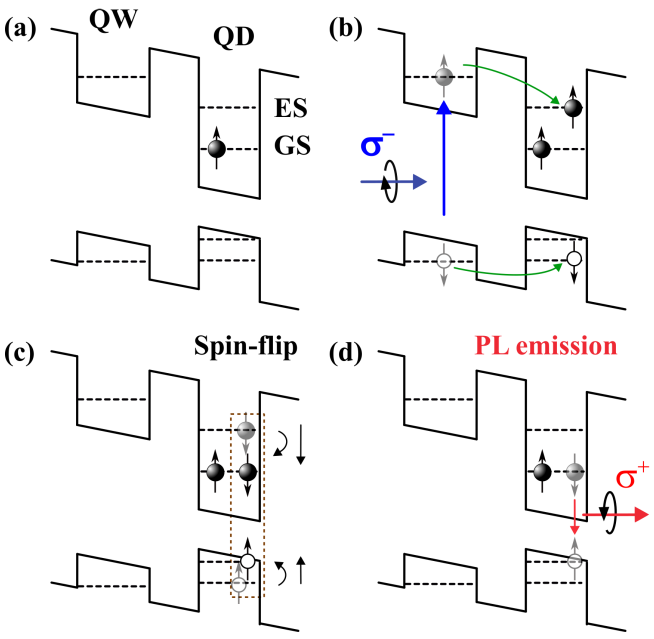

Figure 13. A schematic drawing of the spin-flip process to explain the circularly polarized PL with negative CPDs, observed in the present QW/QDs coupled nanostructure.

For simplicity, I assume that one QD is occupied by one spin-polarized residual electron at the GS [Fig. 13 (a)]. An electron-hole pair in the QW can then be transferred into the QD-ES after the QW excitation via tunneling. The subsequent relaxation to the GS inside the QD can be blocked by the residual electron due to Pauli blocking if this residual electron has a parallel-spin orientation to the latter injected electron (b). Therefore, the electron-hole pair occupies the ES and the electron spin in this ES induces a simultaneous spin-flip transition [26]. After this spin-flip transition, the anti-parallel electron and hole spins for the first residual electron can relax to the GS (c). This anti-parallel electron-hole pair at the GS can recombine and the cross-circular polarization PL (σ^+) is emitted. As a result, the negative CPD (anti-parallel spin for the initial one in the QW) appears (d).

Figure 14 shows an averaged CPD value in the un-doped GS-PL as a function of excitation light power (P_{exc}).

At 1.0 V, high values of positive CPD are observed in a low P_{exc} region less than 160 μW and then gradually decrease toward 0 with increasing P_{exc}. In contrast, a negative CPD significantly develops at 0 V with increasing P_{exc} in this low P_{exc} region, reaching the maximum negative CPD at P_{exc} = 160 μW. Beyond 160 μW, this negative CPD tends to gradually approach 0 with increasing P_{exc}. The former P_{exc} dependence of the positive

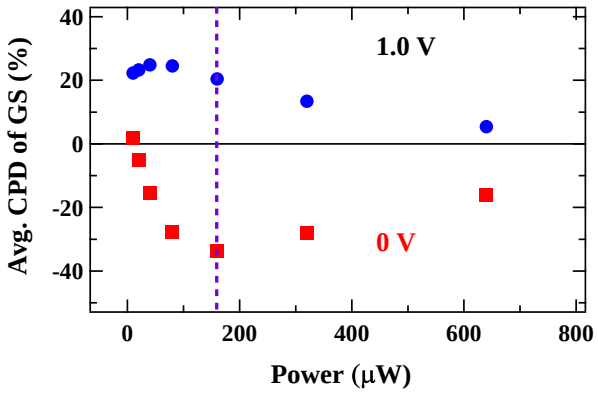

Figure 14. Averaged CPD value in the QD-GSs (1.27–1.29 eV) as a function of excitation light power under σ^- excitation at 4 K with bias voltages of 0 V (a red closed square) and 1.0 V (a blue closed circle).

CPD at 1.0 V can be well explained by a state filling effect in the QD. Spin-polarized electrons can be smoothly injected from the QW into the QDs under relatively low excitation-power conditions. By increasing excitation power, the majority (co-circular) spin states in the QD ensemble can be fully occupied and further spin injection ceases due to Pauli spin blocking [11, 12]. However, the minority spins can be continuously injected causing the spin polarization in the QD ensemble to decrease [9, 10]. According to this spin-flip scenario, the initial development of the negative CPD with increasing P_{exc} at 0 V can be reasonably explained by increasing the residual electron occupation at QD-GSs. Further suppression of this negative CPD as P_{exc} increases beyond 160 μW can also be understood by multiple electron-spin scattering among several QD-ESs in the QDs. This complicated scattering randomize the total spin polarization [28]. We have observed the existence of optimum excitation power for achieving the maximum value of negative CPD, as shown in Fig. 14. Therefore, the degree of spin polarization for both spin polarities. As a result, spin switching efficiency can be optimized by the combination of excitation-spin density and external bias.

5.2 Effects of *p*-doping in QDs

Figures 15 shows effects of *p*-doping on the CPD value of the QD-PL. Positive CPD values ranging from 20% to 30% were observed with positive bias application for all samples, indicating efficient spin injection from the QW.

The strong negative CPD region around 0 V is observed in the un-doped and *p*-doped sample with a lower Be concentration, as shown in Fig. 15 (a). This bias region with negative CPDs is largely affected by heavy *p*-doping in QDs, as shown in (c). The biases exhibiting the negative CPD properties shift to the more nega-

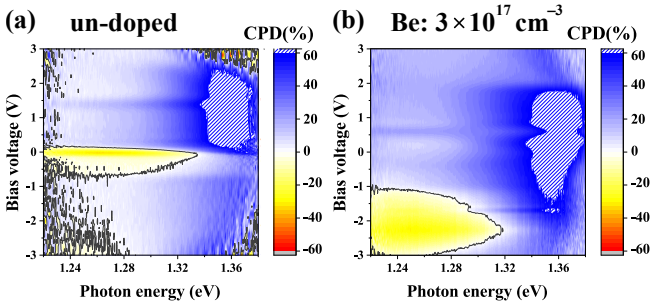

Figure 15. Contour plots of a CPD value of the QD-PL at 4 K as functions of photon energy and bias voltage in (a) the un-doped QD, (b) low-concentration *p*-doped QD, and (c) highly *p*-doped samples. A blue hatched area corresponds to the region with positive CPD $\geq 60\%$.

tive bias side and this bias region becomes significantly broader. Excess holes provided by the *p*-doping can prevent to form negative trions. Therefore, stronger negative bias application is necessary to induce the negative trion formation with the negative CPD. The broad bias region indicating this negative CPD can be explained by inhomogeneous distribution of the number of doped hole in the QD ensemble.

6. Conclusion

Based on my research work, electric-field effects on optical electron-spin injection in QW/QDs coupled nanostructures have been elucidated, as follows:

1: Efficient electron-spin injection from the QW to the ground state (GS) of the QD was found by changing the electric field strength.

After the spin injection, parallel spin states to the initial spin direction in the QW were observed in QDs with wide bias range as a result of the efficient spin injection. The most important finding is the existence of specific bias (+1.2 V) showing the highest positive CPD values (>39%) sufficiently identifiable from the background positive CPDs (∼20%), corresponding to normal spin injection.

2: The spin-injection polarity can be controlled by applying an external bias.

Significant electric-field effects on the reversal of spin polarity were observed at the QD-GS (CPD $\sim -40\%$) in the spin-injection process from the QW. The tunneling rate of an electron is different from that of a hole, which situation largely depends on the electric field strength owing to electric-field induced modifications of the coupled QD-QW potential. This results in negative trions in the QDs with anti-parallel electron spins to the initial ones in the QW, which is supported by a significant effect of *p*-doping into the QDs. The CPD of both spin polarities can be optimized by excitation-spin density, in addition to the electric field strength.

References

[1] L. E. Brus. *The Journal of Chemical Physics*, **79**(11):5566, (1983).

[2] B. L. Liang, Q. Yuan, L. L. Su, Y. Wang, Y. N. Guo, S. F. Wang, G. S. Fu, E. Marega, Y. I. Mazur, M. E. Ware, and G. Salamo. *Optics Express*, **26**(18):23107, (2018).

[3] M. I. Dyakonov. *Spin physics in semiconductors*. Springer, (2008).

[4] H. Drexler, D. Leonard, W. Hansen, J. P. Kotthaus, and P. M. Petroff. *Physical Review Letters*, **73**(16):2252, (1994).

[5] A. P. Alivisatos. *Science*, **271**(5251):933, (1996).

[6] Y. Shirasaki, G. J. Supran, M. G. Bawendi, and V. Bulović. *Nature Photonics*, **7**(1):13, (2013).

[7] Y. X. Yang, Y. Zheng, W. R. Cao, A. Titov, J. Hyvonen, J. R. Manders, J. G. Xue, P. H. Holloway, and L. Qian. *Nature Photonics*, **9**(4):259, (2015).

[8] L. Qian, Y. Zheng, J. G. Xue, and P. H. Holloway. *Nature Photonics*, **5**(9):543, (2011).

[9] T. Kiba, X. J. Yang, T. Yamamura, Y. Kuno, A. Subagyo, K. Sueoka, and A. Murayama. *Applied Physics Letters*, **103**(8):082405, (2013).

[10] T. Yamamura, T. Kiba, X. J. Yang, J. Takayama, A. Subagyo, K. Sueoka, and A. Murayama. *Journal of Applied Physics*, **116**(9):094309, (2014).

[11] T. Amano, T. Sugaya, and K. Komori. *Applied Physics Letters*, **89**(17):171122, (2006).

[12] A. Higo, T. Kiba, Y. Tamura, C. Thomas, J. Takayama, Y. Wang, H. Sodabanlu, M. Sugiyama, Y. Nakano, I. Yamashita, A. Murayama, and S. Samukawa. *Scientific Reports*, **5**:9371, (2015).

[13] R. Fiederling, M. Keim, G. Reuscher, W. Ossau, G. Schmidt, A. Waag, and L. W. Molenkamp. *Nature*, **402**(6763):787, (1999).

[14] O. M. J. Van't Erve, G Kioseoglou, A. T. Hanbicki, C. H. Li, and B. T. Jonker. *Applied Physics Letters*, **89**(7):072505, (2006).

[15] G. Itskos, E. Harbord, S. K. Clowes, E. Clarke, L. F. Cohen, P. Murray, R .and Van Dorpe, and W. Van Roy. *Applied Physics Letters*, **88**(2):022113, (2006).

[16] M. Paillard, X. Marie, P. Renucci, T. Amand, A. Jbeli, and J. M. Gérard. *Physical Review Letters*, **86**(8):1634, (2001).

[17] S. Hiura, K. Itabashi, K. Takeishi, J. Takayama, T. Kiba, and A. Murayama. *Applied Physics Letters*, **114**(7):072406, (2019).

[18] Y. Masumoto, S. Oguchi, B. Pal, and M. Ikezawa. *Physical Review B*, **74**(20):205332, (2006).

[19] Y. Chye, M. E. White, E. Johnston-Halperin, B. D. Gerardot, D. D. Awschalom, and P. M. Petroff. *Physical Review B*, **66**(20):201301, (2002).

[20] K. Takeishi, S. Hiura, J. Takayama, K. Itabashi, M. Urabe, A. Washida, T. Kiba, and A. Murayama. *Physical Review Applied*, **10**(3):034015, (2018).

[21] X. J. Yang, T. Kiba, T. Yamamura, J. Takayama, A. Subagyo, K. Sueoka, and A. Murayama. *Applied Physics Letters*, **104**(1):012406, (2014).

[22] S. L. Chen, T. Kiba, X. J. Yang, J. Takayama, and A. Murayama. *Applied Physics Letters*, **108**(15):152103, (2016).

[23] S. L. Chen, T. Kiba, X. J. Yang, J. Takayama, and A. Murayama. *Journal of Applied Physics*, **119**(11):115701, (2016).

[24] Y. Puttisong, Y. Q. Huang, I. A. Buyanova, X. J. Yang, A. Subagyo, K. Sueoka, A. Murayama, and W. M. Chen. *Applied Physics Letters*, **105**(13):132106, (2014).

[25] F. Meier and B. P. Zakharchenya. *Optical orientation*. Elsevier, (2012).

[26] B. Pal, S. Y. Verbin, I. V Ignatiev, M. Ikezawa, and Y. Masumoto. *Physical Review B*, **75**(12):125322, (2007).

[27] M. W. Taylor, P. Spencer, and R. Murray. *Applied Physics Letters*, **106**(12):122404, (2015).

[28] A. Shabaev, E. A. Stinaff, A. S. Bracker, D. Gammon, A. L. Efros, V. L. Korenev, and I. Merkulov. *Physical Review B*, **79**(3):035322, (2009).